Forcing of a flame by a periodic flow in a Hele-Shaw burner

Basile Radisson, Bruno Denet, Christophe Almarcha

Forcing of a flame by a periodic flow in a Hele-Shaw burner

Basile Radisson, Bruno Denet and Christophe Almarcha
Aix Marseille Université, CNRS, Centrale Marseille, IRPHE UMR 7342, 13384 Marseille, France
(Dated: January 3, 2023)

The parametric forcing of premixed flames is observed here in the geometry of a Hele-Shaw burner. Using a vibroacoustic coupling, we are able to study the thresholds of the parametric flattening (where the flame wrinkles are suppressed) and the parametric instability (where the flame wrinkles oscillate at twice the acoustic period) and compare the measured values to a low frequency theory. It is shown that the dependency of the parametric threshold with equivalence ratio is lower than predicted, suggesting that the Markstein lengths are frequency-dependent, and that the flattening threshold is independent of the Markstein number and of the non-dimensional forcing frequency, in agreement with the Bychkov limit.

I. INTRODUCTION

The interaction of a flame with acoustics is a fundamental problem in combustion. It is traditionally studied to understand and prevent the formation of thermo-acoustic instabilities. Acoustic waves are also useful to analyze how flames respond to time dependent flows. In particular, in combustion models where the flame is described as a discontinuity of the flow, the local speed of propagation of the flame front $\mathbf{w}$ is related to the speed of the upcoming flow $\mathbf{u_1}$ by a kinematic relation of the form [1–4]:

$$(\mathbf{u_1} - \mathbf{w}) \cdot \mathbf{n} = u_L - \mathcal{L}_I \frac{u_L}{R} + \mathcal{L}_{II} \mathbf{n} \cdot \nabla \mathbf{u_1} \cdot \mathbf{n}, \tag{1}$$

where $\mathbf{n}$ is the normal vector to the flame front (directed towards the burnt gases), u_L is the laminar flame speed, R is the local radius of curvature of the flame front, $\mathbf{n} \cdot \nabla \mathbf{u_1} \cdot \mathbf{n}$ is the normal-normal component of the rate-of-strain tensor and $\mathcal{L}_I$ and $\mathcal{L}_{II}$ are the Markstein lengths. These two parameters are key quantities in combustion models. They express the role of transport phenomena happening in the thickness of the flame and allow them to be taken into account while still considering the flame as a flow discontinuity. Their expression is traditionally obtained through asymptotic analysis of the internal structure of the flame under the assumption that the typical spatial and time scales of the incident flow are large compared to the transit time τ_L and thickness d_L of the flame, respectively [5–7]. However, when the time scales associated with the flow are no longer large in comparison to the transit time of the flame, its typical response to curvature and strain is likely to be modified. This question was first addressed theoretically by Joulin [8] in the framework of a constant density model. He demonstrated that the flame response to stretch is indeed frequency dependent by performing an asymptotic analysis of the internal structure of the flame and considering a curvature and normal-normal component of the rate of strain tensor that vary periodically in time at a frequency $\widetilde{\omega}_a$. More precisely, when $\widetilde{\omega}_a$ is increased, $\mathcal{L}_{II}$ monotonically decreases until the flame response to strain completely disappears at high forcing frequency. This is due to a memory effect that makes the flame insensitive to hydrodynamic stretch when the latter occurs on a too small time scale (compared with τ_L). The flame does not have time to see the flow variations occurring at times scales that are small compared to the transit time. The diffusive mechanisms are no longer effective on these short time scales for the same reason. Therefore, the Lewis number component of $\mathcal{L}_I$ vanishes at high frequency for which all the flames behave as if $Le = 1$. These analytical results were qualitatively confirmed later in the more realistic variable density framework [9].

From a numerical or experimental standpoint, there are only a few studies that have addressed the frequency dependence of Markstein lengths. Indeed, due to the fact that their value depends on the position of the adopted surface of reference within the flame, their direct measurement is made very complicated [10, 11]. An alternative is to perform indirect measurement of their value by analyzing the dynamics of a flame submitted to a periodic flow. As first suggested by Markstein [12], when advected by a periodic flow, the flame front is described by a parametric oscillator equation. As such, parametric restabilization and parametric resonance can be observed. Searby and Rochwerger [13] have proposed a refined version of Markstein's theory that allows the prediction of the parametric restabilization and parametric resonance thresholds in terms of the amplitude of the acoustic wave and the wavenumber of the perturbation. In their study they have compared these theoretical thresholds to experimental measurements obtained for hydrocarbon flames propagating downwards in a tube; these flames were forced by an acoustic wave that was generated by a speaker positioned at the bottom of the tube. Their measurements seem to corroborate Joulin's theory: at high frequency, all the flames seem to respond in the same way, independently of their chemical composition. Similar observations were obtained in [14] with threshold measurements obtained from DNS.

In the present paper, we propose to supplement these previous studies by presenting new experimental measurements of these threshold values on flames propagating in a Hele-Shaw burner. This type of burner has been extensively exploited in recent studies for its potential applications in micro combustion devices and the easy visualization of flame dynamics that it offers [15–21]. Until recently, it was still not clear if the same parametric behavior could be obtained in such a device due to the confined geometry associated with this type of burner. The viscous losses at the walls of the burner were shown to inhibit the occurrence of the standard thermo-acoustic instability [19, 22]. In a recent study, we demonstrated that parametric restabilization and parametric resonance can be observed in this kind of apparatus and we uncovered a new type of coupling between the flame propagation and the structural modes of the burner [23]. Here we propose to exploit this coupling mechanism to perform measurements of restabilization and parametric thresholds. For this purpose, one of the walls of the burner is forced with a shaker in order to excite one of its eigen modes. As demonstrated in [23], this in turn produces an oscillating flow in the burner cavity that interacts with the flame propagation in the same way as in the tube of the Searby and Rochwerger experiment. Our apparatus is more versatile than that in the Searby and Rochwerger experiment for two reasons : i) due to its particular geometry the dynamics of the flame are quasi-2D and easier to visualize. This allows us to define precisely the instant when a threshold is crossed. Moreover, it is possible to design very large Hele-Shaw burners and determine accurately the restabilization threshold ($\widetilde{k}_I^*$,$\widetilde{u}_I^*$ in the following) corresponding to large wavelengths. This was more difficult with

their tube experiments and so they focused only on the parametric instability threshold ($\widetilde{k}^*_{II}$,$\widetilde{u}^*_{II}$ in the following). In this paper we will see that studying this restabilization threshold provides interesting information on the flame response. ii) the eigen mode of the structure can be easily varied by changing the material or geometrical properties of the walls of the Hele-Shaw burner, which allows us to study the flame response to a large range of frequency with the same apparatus. The present paper is organized as follows: in §II we introduce the experimental apparatus and the procedure employed to perform these measurements. In §III we briefly present the Searby and Rochwerger theory and the main properties of the parametric oscillator equation describing the flame dynamics. Our experimental results are then presented and compared to the theory in §IV and we finally discuss these results, emphasizing particularly the discrepancy between our measurements and the theory.

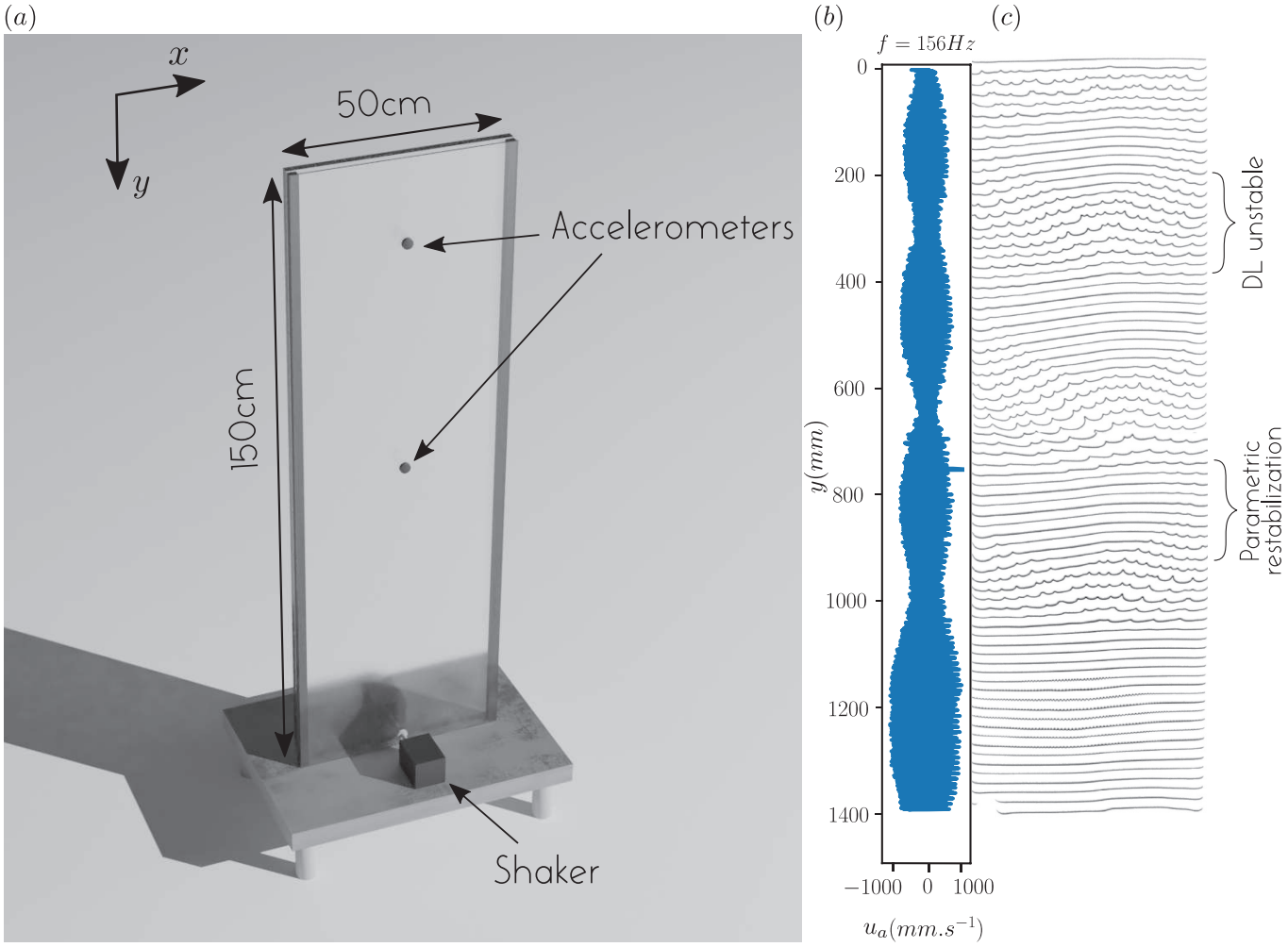

Figure 1. Experimental apparatus. A. The flame propagates downwards in a Hele-Shaw burner composed of two borosilicate glass plates oriented vertically and separated by a 5 mm gap. The burner cavity is closed on the sides and at the bottom and open at the top. The eigenmodes of one of the plates are forced using a shaker and the resulting vibrations are recorded using two accelerometers positioned on the plate (see [23] for details). B. The oscillations of the plates generate an oscillating flow in the burner cavity. Here we plot the vertical component of the flow speed u_a (on the horizontal axis) in terms of the vertical position in the Hele-shaw burner y (on the vertical axis where the zero corresponds to the top end of the burner). Moving downwards in the burner, we observe a succession of areas with a low amplitude oscillating flow (nodes) and areas with a large amplitude oscillating flow (antinodes). These nodes and antinodes of the flow speed correspond to nodes and antinodes of the plate vibrations [23]. C. When propagating downwards, the flame undergoes a periodic oscillating flow with different acoustic amplitude depending on the position in the tube, and exhibits parametric restabilization and/or parametric destabilization.

II. PARAMETRIC FORCING OF A PREMIXED FLAME

The Hele-Shaw burner used in this study is composed of two borosilicate glass plates (Young modulus $E = 69GPa$) separated by a $5mm$ gap. The two plates are $1500mm$ in height and $500mm$ in width. The burner cavity is closed on the sides and at the bottom and open at the top. The oscillating flow is generated by enforcing a structural mode of the burner with a shaker attached to one of the walls (see Fig. 1A). The glass plate of the Hele-Shaw burner can be switched between $h = 5mm$ and $h = 19mm$ thicknesses. This modifies the bending stiffness of the plate and allows for expansion of the range of frequencies we can study. For each experiment reported hereafter, the shaker frequency is adjusted to an eigenmode of the plate in order to generate large bending oscillations (see [23] for details). The deformations of the wall induce volume variation in the burner cavity. This in turn generates vertical flow oscillations with variable amplitude depending on the vertical position in the burner. A typical profile of the amplitude of the vertical flow oscillations u_a is presented on Fig. 1B. The bending mode shape leads to non-homogeneous amplitude of the oscillating velocity with a succession of low velocity amplitude regions (nodes) and high velocity amplitude regions (antinodes). When a flame, ignited at the top of the burner, propagates downwards through this oscillating flow, its dynamics are strongly influenced. A typical space time diagram of the obtained flame is presented on Fig. 1. We notice that the flame is wrinkled when crossing low flow velocity regions, but it is flattened when passing through regions where the amplitude of the oscillating flow is large. This is a typical observation of a parametric flattening of a Darrieus-Landau (DL) unstable flame. These dynamics are correctly described by the following Searby Rochwerger theory.

III. SEARBY ROCHWERGER THEORY

A. The equivalent parametric oscillator

This theory, following the pioneering idea of Markstein [12], considers that the coupling with the flame is essentially controlled by the acceleration. This is contrary to other models where the coupling is caused by the pressure and leads to a pulsating acceleration term added to the gravity in the equation introduced in [7] (eq. (37)). When all the lengths are rescaled by the flame thickness d_L and the time is rescaled by the transit time $\tau_L = d_L/u_L$, the following non-dimensional oscillator equation for the vertical coordinate of the front is obtained

$$\frac{\partial^2 \widehat{\Phi}}{\partial \widetilde{t}^2} + 2c\frac{\partial \widehat{\Phi}}{\partial \widetilde{t}} + \left(a + a_1 \cos(\widetilde{\omega}_a \widetilde{t})\right) \widehat{\Phi} = 0, \tag{2}$$

where $\widehat{\Phi}$ is the amplitude of the mode $\widetilde{k}$, $\widetilde{t}$ is the non-dimensional time and $\widetilde{\omega}_a$ is the non-dimensional pulsation of the acoustic oscillation. c , a and a_1 are given by :

$$c = \widetilde{k}\frac{\left(1 + \widetilde{k}(Ma - \mathcal{J})/(1-\gamma)\right)}{(2-\gamma) + \gamma\widetilde{k}\,(Ma - \mathcal{J}/\gamma)} \tag{3}$$

$$\begin{aligned} a = &\left\{ \frac{\gamma}{Fr^2}\widetilde{k} - \frac{\gamma}{1-\gamma}\widetilde{k}^2\left(1 + \frac{1-\gamma}{Fr^2}\left(Ma - \frac{\mathcal{J}}{\gamma}\right)\right)\right. \\ &\left. + \frac{\gamma}{1-\gamma}\widetilde{k}^3\left(\lambda_2 + (2+\gamma)\frac{Ma}{\gamma} - \frac{2\mathcal{J}}{\gamma} + (2Pr-1)\,\mathcal{H}\right)\right\} \\ &\Big/\left\{ (2-\gamma) + \gamma\widetilde{k}\,(Ma - \mathcal{J}/\gamma)\right\} \end{aligned} \tag{4}$$

$$a_1 = \frac{\gamma\widetilde{k}\widetilde{u}_a\widetilde{\omega}_a\left(1 - \widetilde{k}\,(Ma - \mathcal{J}/\gamma)\right)}{(2-\gamma) + \gamma\widetilde{k}\,(Ma - \mathcal{J}/\gamma)} \tag{5}$$

where $\gamma = (\rho_u - \rho_b)/\rho_u$ depends on the density in the burned and unburned gases, λ_2 is the non-dimensional thermal conductivity evaluated at burnt gases temperature, $Ma = \mathcal{L}_I/d_L = \mathcal{L}_{II}/d_L$ is the Markstein number (which is unique in the case of simple chemistry and when the front position is defined as the position of the reacting sheet as done in [7]), $Fr = u_L/\sqrt{gd_L}$ is the Froude number associated with flame propagation, $Pr = \nu/D_{th}$ (with ν the momentum diffusivity and D_{th} the thermal diffusivity) is the Prandtl number evaluated at fresh gases temperature

and $\widetilde{u}_a = u_a/u_L$ is the reduced acoustic velocity.
The integrals $\mathcal{H}$ and $\mathcal{J}$ are given by :

$$\mathcal{H} = \int_0^1 \lambda_2 - \lambda(\theta) d\theta \tag{6}$$

$$\mathcal{J} = \frac{\gamma}{1-\gamma} \int_0^1 \frac{\lambda(\theta)}{1+\theta\gamma/(1-\gamma)} d\theta \tag{7}$$

where $\lambda(\theta)$ is the thermal conductivity evaluated at reduced temperature θ normalized by the thermal conductivity λ_1 in fresh gas, and λ_2 is the conductivity in burned gas.

Setting :

$$z = \frac{1}{2}\widetilde{\omega}_a \widetilde{t}, \tag{8}$$

$$\mathcal{Y}(z) = \widetilde{\phi}(\widetilde{t}) \exp(c\widetilde{t}), \tag{9}$$

$$\widetilde{a} = \frac{4\left(a - c^2\right)}{\widetilde{\omega}_a^2}, \tag{10}$$

$$q = -\frac{2a_1}{\widetilde{\omega}_a^2}, \tag{11}$$

equation (2) is reduced to the so called Mathieu equation :

$$\frac{d^2\mathcal{Y}}{dz^2} + (\widetilde{a} - 2q\cos(2z))\,\mathcal{Y} = 0 \tag{12}$$

Floquet theory predicts solutions in the form :

$$\mathcal{Y}(z) = \exp(\mu z)\psi(z) + \exp(-\mu z)\psi(-z) \tag{13}$$

Where ψ is a 2π-periodic function and μ is the Floquet exponent (also called characteristic exponent). Thanks to (13), the stability condition of Mathieu equation solutions is made explicit : If $Re(\mu) > 0$, $\mathcal{Y}(z)$ grows exponentially with z (unstable), otherwise the solution is stable ($Re(\mu) \leq 0$). Typical stability diagrams for $\mathcal{Y}(z)$ can be seen in [24] for example s???.
The stability condition for $\widehat{\Phi}(t)$ is then obtained from (8) and (9). The flame front is stable if $Re(\mu) \leq 2c/\widetilde{\omega}_a$ and unstable if $Re(\mu) > 2c/\widetilde{\omega}_a$. As $\widetilde{a}$ and q depend on the wavenumber of the perturbation $\widetilde{k}$, on the physico-chemical parameters of the flame and on the forcing parameters ($\widetilde{\omega}_a$, $\widetilde{u}_a$), their physical meaning is difficult to understand. Therefore, in the following, the stability diagrams for $\widehat{\Phi}$ will be shown in the $(\widetilde{k}, \widetilde{u}_a)$ plan. Typical diagrams are plotted on Fig. 2 for different values of $\widetilde{\omega}_a$, Fr, Ma. Here we use the same parameters as those used in [25] Fig. 1, which are restated here:

$$Pr = 0.689 \qquad \gamma = 0.822 \qquad \lambda_2 = 3.19 \qquad \mathcal{H} = 0.96 \qquad \mathcal{J} = 3.33 \tag{14}$$

Other parameters are given on the plots. To obtain these diagrams, for each set of parameters $(\widetilde{\omega}_a, Fr, Ma)$, the corresponding values for $\widetilde{a}$, q and $\kappa = 2c/\widetilde{\omega}_a$ are computed. The Floquet exponent $\mu(\widetilde{a}, q)$ is then obtained numerically [26] and the stability condition $Re(\mu(\widetilde{a}, q)) \leq \kappa(\widetilde{a}, q)$ is verified. The process is repeated for each set of parameters $(\widetilde{k}, \widetilde{u}_a)$. With the above parameters, the obtained diagrams agree well with those obtained in [25]. This validates our method to compute the characteristic exponents. On diagram B and C, a third unstable zone, not visible in [25], is observed (see also [27, 28]). It corresponds to the second region of unstable solutions visible on the typical Mathieu stability diagram (see [24]). This second parametric resonance is never observed (at the parametric threshold) in our experiments, as the acoustic threshold associated with it is always higher than that associated with the first resonance.

We now focus on the first two regions. The first one corresponds to the zone where the flame is Darrieus-Landau unstable. For $\widetilde{u}_a = 0$ (no forcing), this region corresponds to the range of unstable wavenumbers given by the dispersion relation obtained in [7]. As $\widetilde{u}_a$ is increased, the range of unstable wavenumbers narrows until this zone completely disappears for $\widetilde{u}_a = \widetilde{u}_I^*$. At this threshold intensity, there is only one DL unstable wavenumber $\widetilde{k}_I^*$. The second region

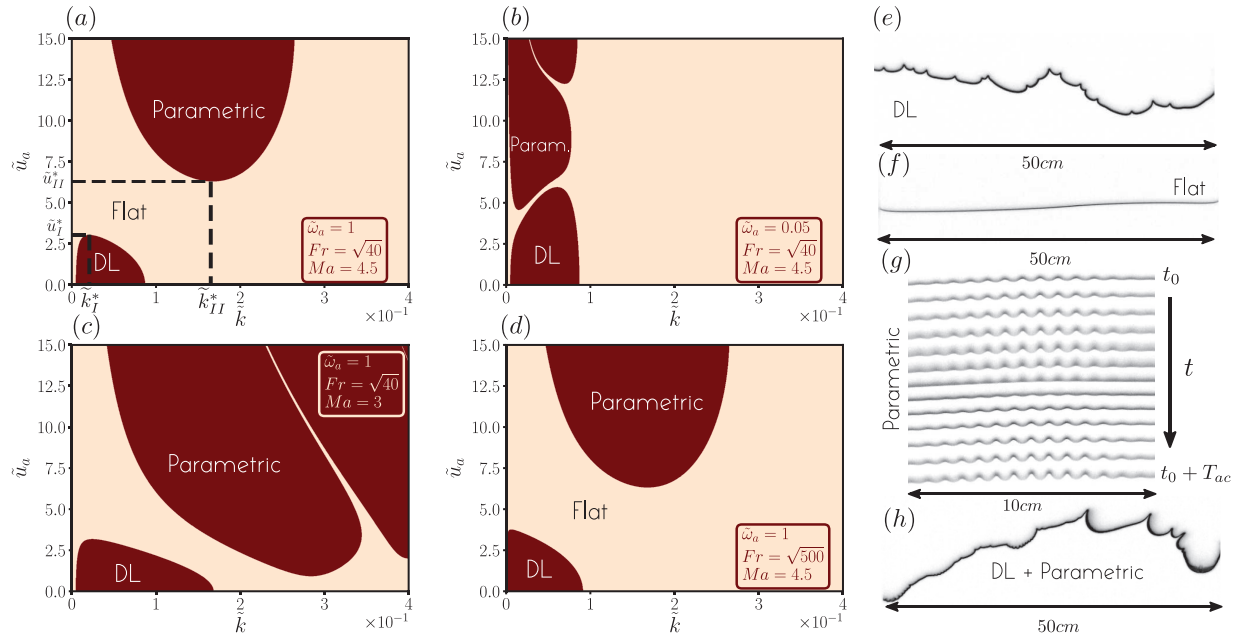

Figure 2. Stability diagrams for different set of parameters and their corresponding regimes of propagation. For a given set of parameters where $\widetilde{u}_I^* < \widetilde{u}_{II}^*$ (see **A.** and **D.** for examples), three different scenarios of propagation can be observed depending on the acoustic amplitude $\widetilde{u}_a$: (i) if $\widetilde{u}_a < \widetilde{u}_I^*$, the flame is DL unstable and exhibits characteristic wrinkling with cusps pointing towards the burnt gases (see **D.**), (ii) if $\widetilde{u}_I^* < \widetilde{u}_a < \widetilde{u}_{II}^*$, all the wavenumbers are stable and parametric flattening is observed (see **F.**), (iii) if $\widetilde{u}_a > \widetilde{u}_{II}^*$, a typical parametric instability is observed with patterns pulsating at half the forcing frequency $\widetilde{\omega}_a$. On frame **G.** the evolution of a parametrically excited front is represented over one full accoustic period (from top to bottom). We note that at the end of the period the minima and maxima of the front have exchanged positions. After another acoustic period, the minima and maxima would get back to their original position (The period of the pattern is twice the acoustic period). On the other hand, if for a given set of parameters, $\widetilde{u}_{II}^* < \widetilde{u}_I^*$, there is no parametric restabilization zone (see **B.** and **C.**). Instead DL instability and parametric instability may coexist for a certain range of $\widetilde{u}_a$ (see **H.** where one can note the DL (large wavelength) and the parametric (small wavelength) instabilities).

corresponds to the first parametric resonance of the oscillator equation associated with the flame dynamics. This zone appears for a non zero acoustic intensity $\widetilde{u}_a = \widetilde{u}_{II}^*$ at a wave number $\widetilde{k}_{II}^*$. As the forcing intensity is increased, this zone becomes larger, leading to a wider range of unstable wavenumbers. As can be seen on Fig. 2, the thresholds $\widetilde{u}_I^*$ and $\widetilde{u}_{II}^*$ depend on the flame parameters and on the forcing frequency.
If for a given set of parameters, $\widetilde{u}_{II}^* > \widetilde{u}_I^*$ (for example, in Fig. 2A and 2D), three different scenarios may be observed, depending on the forcing intensity $\widetilde{u}_a$: (i) If $\widetilde{u}_a < \widetilde{u}_I^*$, the flame is Darrieus-Landau unstable (see Fig. 2E). (ii) If $\widetilde{u}_I^* < \widetilde{u}_a < \widetilde{u}_{II}^*$, the DL instability disappears and the flame is flattened (see Fig. 2F). We will call this zone the restabilization zone. (iii) Finally, if $\widetilde{u}_a > \widetilde{u}_{II}^*$, a parametric instability is observe and the flame front exhibits a cellular aspect with structures oscillating at a frequency twice smaller than the forcing frequency (see Fig. 2G).
Otherwise, if $\widetilde{u}_{II}^* < \widetilde{u}_I^*$ there is no restabilization zone (see Fig. 2B and 2C). The DL instability and the parametric one may coexist in the case where $\widetilde{u}_{II}^* < \widetilde{u}_a < \widetilde{u}_I^*$ (see Fig. 2H).

By computing stability diagrams, as the ones presented in Fig. 2, the theoretical thresholds of the parametric flattening (acoustic velocity $\widetilde{u}_I^*$ with wavenumber $\widetilde{k}_I^*$) and parametric instability (acoustic velocity $\widetilde{u}_{II}^*$ with wavenumber $\widetilde{k}_{II}^*$) can be obtained for several sets of parameters.

B. Parametric oscillator properties

Here, we focus on the dependence of the theoretical threshold values $(\widetilde{k}_I^*, \widetilde{u}_I^*)$ and $(\widetilde{k}_{II}^*, \widetilde{u}_{II}^*)$, on the forcing frequency $\widetilde{\omega}_a$ and on the value of the Markstein number. The thresholds are computed numerically using the same procedure as the one used to obtain the diagram of Fig. 2. The Markstein number Ma and the reduced forcing frequency $\widetilde{\omega}_a$ are varied. Other parameters are fixed with the following values (these values correspond to lean propane-air flames

$\varphi = 0.8.$):

$$\begin{array}{lll} Fr = 10.58 & Pr = 0.9 & \gamma = 0.854 \\ \lambda_2 = 2.62 & \mathcal{H} = 0.69 & \mathcal{J} = 1.62 \end{array} \tag{15}$$

1. *Thresholds dependency on Markstein number*

First, the parameters given in (15) and the forcing frequency $\widetilde{\omega}_a$ are fixed and the Ma value is varied from $Ma = 2$ to $Ma = 5.5$. For each Ma value, the bottom point of the parametric zone and the top point of the Darrieus-Landau zone are evaluated numerically. The obtained results are shown on Fig. 3C and 3D for two different values of the

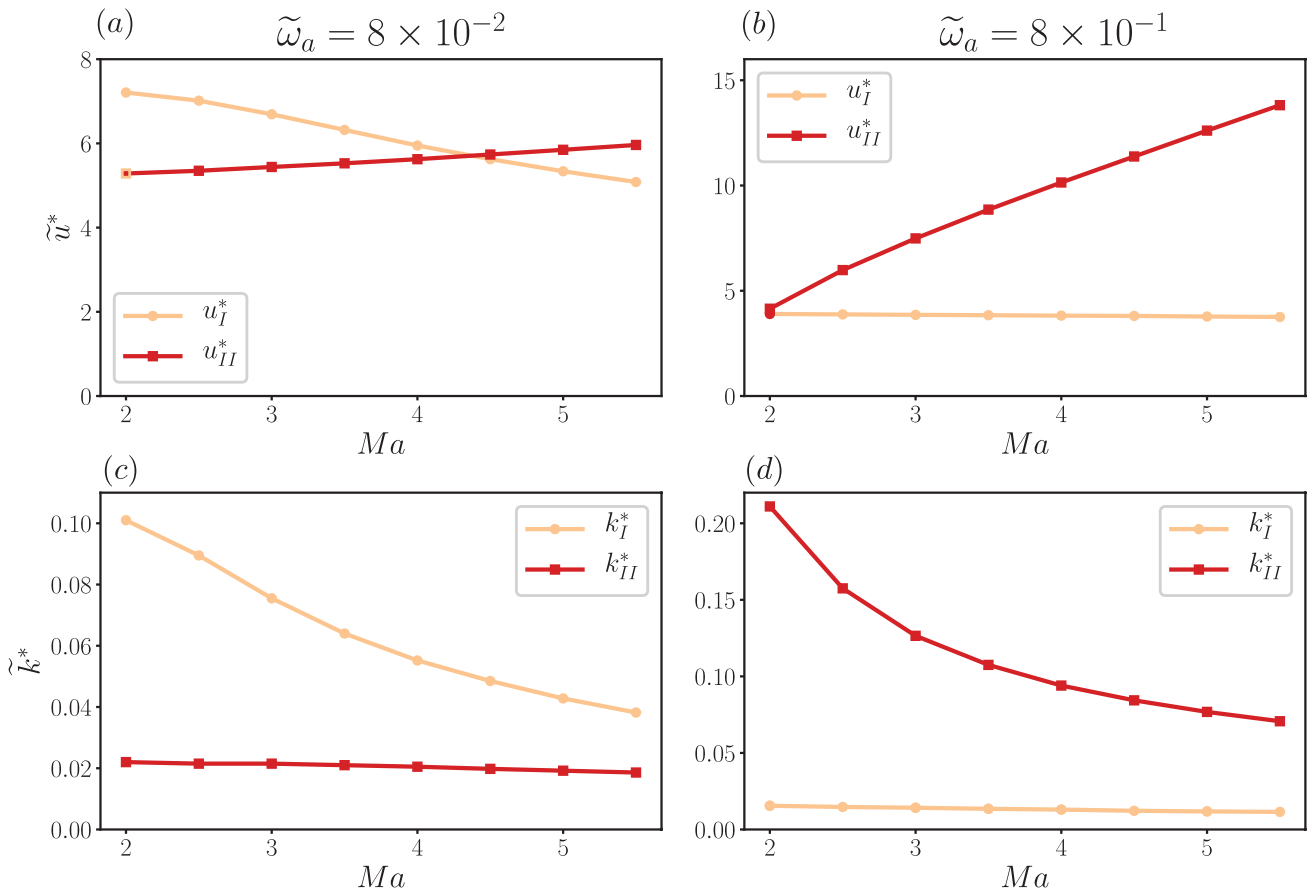

Figure 3. Dependence of the restabilization/parametric thresholds to Ma. A. $\widetilde{u}_I^*$ and $\widetilde{u}_{II}^*$ against Ma at small forcing frequency. B. $\widetilde{u}_I^*$ and $\widetilde{u}_{II}^*$ against Ma at high forcing frequency. C. $\widetilde{k}_I^*$ and $\widetilde{k}_{II}^*$ against Ma at small forcing frequency. D. $\widetilde{k}_I^*$ and $\widetilde{k}_{II}^*$ against Ma at high forcing frequency.

forcing frequency. When Ma increases, both the stabilization and the parametric thresholds drift toward larger wavelengths. This is due to the fact that for larger Ma, the small wavelengths are more damped by diffusive effects. This tendency is weaker for $\widetilde{k}_I^*$ than for $\widetilde{k}_{II}^*$. On the other hand, two opposite trends are observed for $\widetilde{u}_I^*$ and $\widetilde{u}_{II}^*$. When Ma is increased, the restabilization (respectively the parametric) threshold is decreased (respectively increased). The restabilization zone that occurs when $\widetilde{u}_{II}^* > \widetilde{u}_I^*$ is therefore larger at high Ma and tends to be completely suppressed when Ma is decreased at low frequency(see Fig. 3A). This trend is due to the dependency of the damping coefficient c in the oscillator equation (2) on the Markstein number. When Ma decreases, the damping is reduced too, and the parametric zone goes down (for zero damping ($c = 0$) $\widetilde{u}_{II}^* \to 0$). At high frequency (see Fig. 3B) , the variation of $\widetilde{u}_{II}^*$ with Ma is strong whereas the $\widetilde{u}_I^*$ is weakly dependent on Ma. The wavelength at the parametric instability threshold is smaller than that of the DL, provided that the forcing frequency is sufficiently large (see Fig. 3D). However, at

low forcing frequency, and especially at a low Markstein number, the DL wavelength may be smaller than that of the parametric instability (see Fig. 3C).

2. *Thresholds dependence on forcing frequency*

The same kind of analysis is now performed to study the dependency of the threshold values on forcing frequency. The Markstein number is now fixed (three different values are reported) and the reduced forcing frequency is varied over one order of magnitude. This kind of parametric exploration has already been presented in [25] Fig. 4 and in [29] Fig. 11 for the parametric threshold (u^*_{II}, k^*_{II}). Their results are recalled now for the purpose of the following discussion. We also present the restabilization threshold dependency on the forcing frequency; the results are plotted on Fig. 4. As shown, the restabilization threshold $(\widetilde{k}^*_I, \widetilde{u}^*_I)$ is frequency dependent only at small frequency values. This property is consistent with the theory developed by Bychkov in [30], which predicts no frequency dependency for the DL zone (this analysis is asymptotically exact in the limit $\widetilde{\omega}_a \gg \widetilde{k}\sqrt{a}$). On the other hand, the threshold

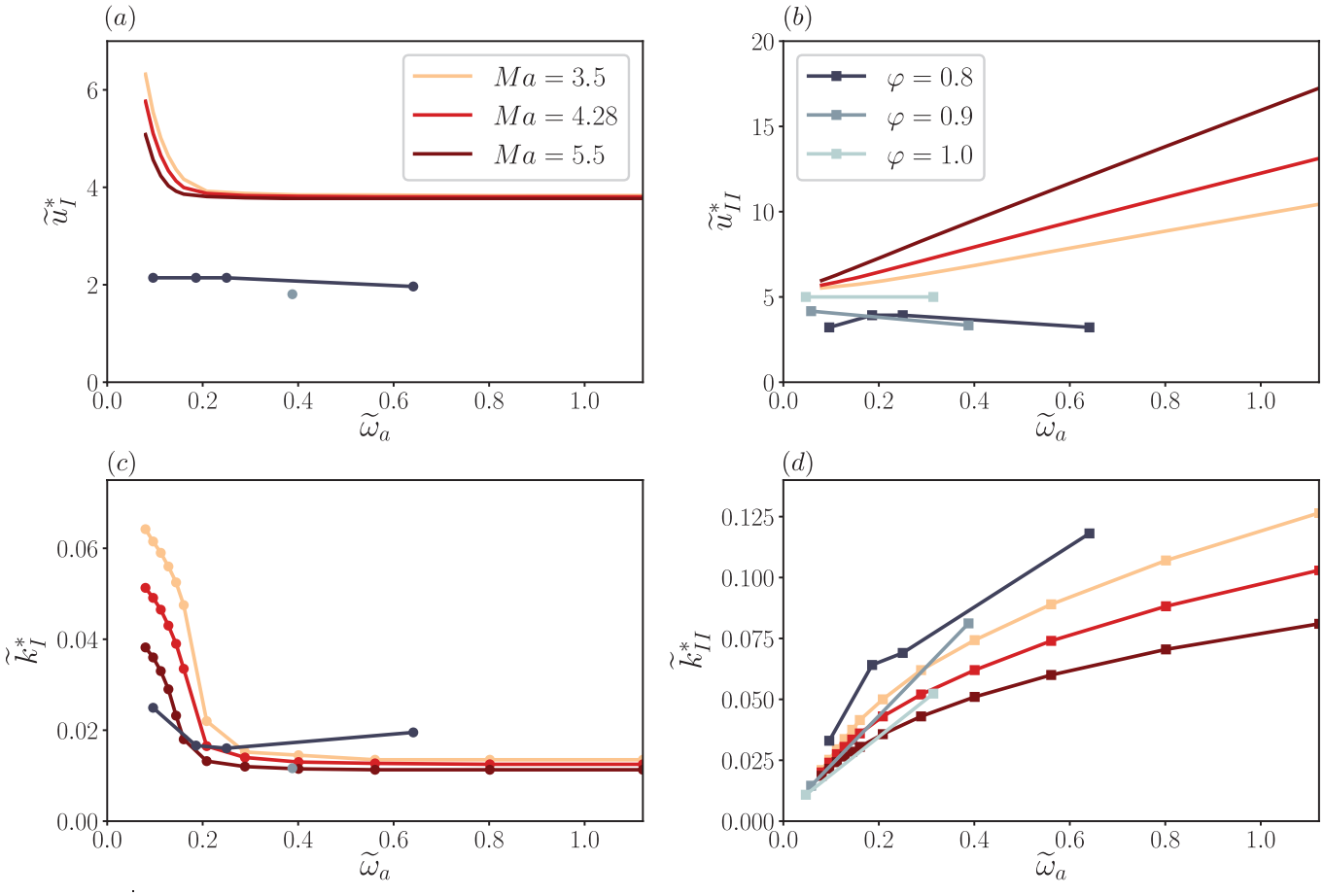

Figure 4. Comparison between experimental and theoretical threshold values with respect to the non-dimensional forcing frequency $\widetilde{\omega}_a$. Theoretical data for different Markstein number values are reported in shades of red and experimental data for different equivalence ratios φ are reported in shades of grey. A. Comparison of the restabilization threshold u^*_I. B. Comparison of the restabilization threshold u^*_{II}. C. Comparison of the last unstable reduced wavenumber k^*_I before restabilization. D. Comparison of the first unstable reduced wavenumber k^*_{II} above the parametric threshold.

of the parametric zone exhibits a strong linear dependence on $\widetilde{\omega}_a$. The variation is even more pronounced when the Markstein number is high. As the theory predicts a linear increasing parametric threshold $\widetilde{u}^*_{II}$ and a constant threshold $\widetilde{u}^*_I$, all flames should exhibit a restabilization zone at high frequency (i.e a range of forcing for which the flame is completely flattened). As we shall see in the following, this is not what we observe in our experiments.

IV. EXPERIMENTAL RESULTS

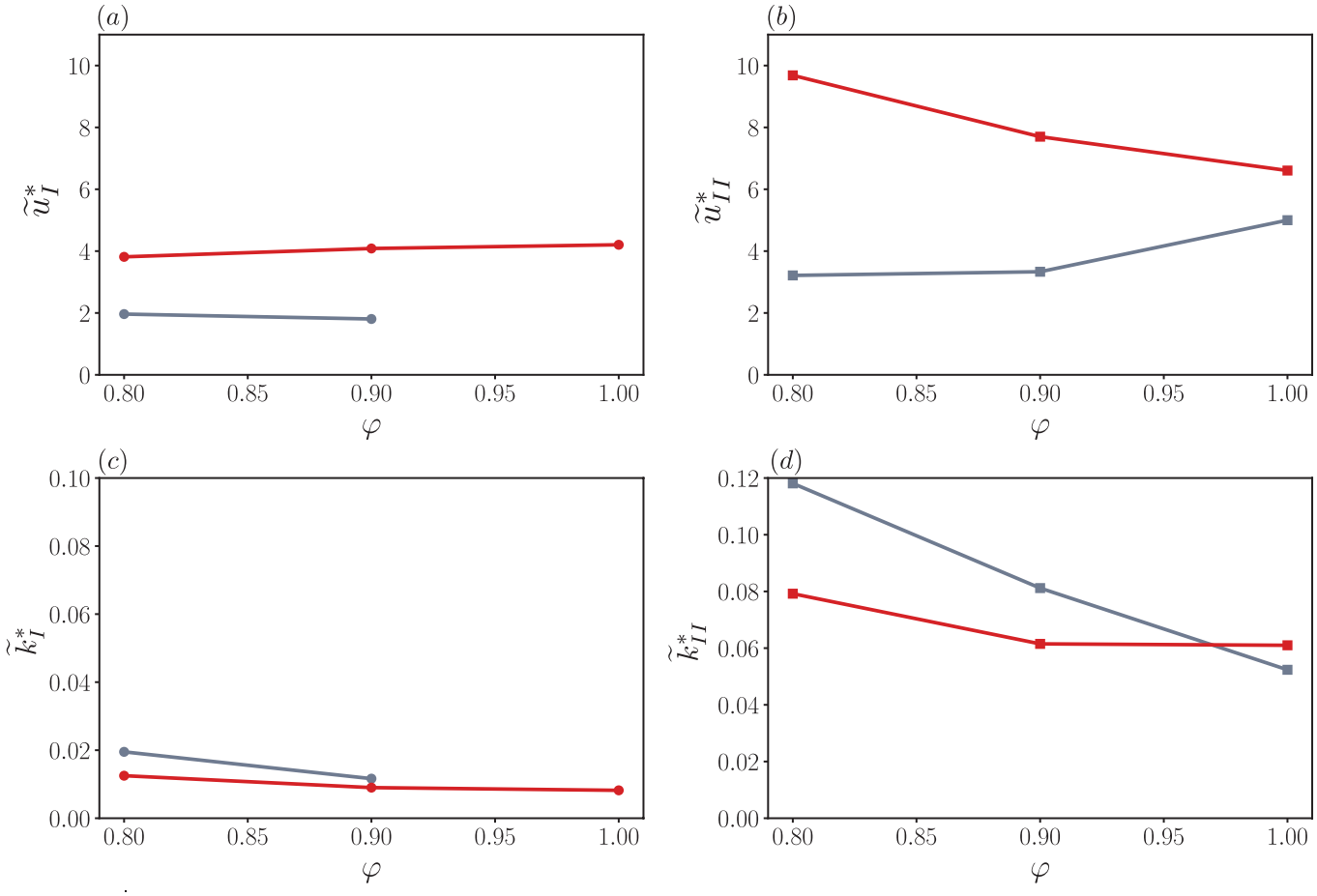

Figure 5. Comparison of experimental thresholds (gray) with those predicted by Searby & Rochwerger theory (red). For the three cases presented here the forcing frequency is $f_{shaker} = 400Hz$. A. Comparison of the restabilization threshold for propane-air flame with different equivalence ratios φ. B. Same for parametric thresholds. C. Comparison of the last unstable wavenumber at the restabilization threshold. D. First unstable wavenumber at the parametric threshold.

As we are interested in measuring the flattening and the parametric thresholds experimentally, we want to analyze flames that admit a restabilisation zone (i.e $u_I^* < u_{II}^*$) so that these thresholds can be measured from a flat front. Lean heavy hydrocarbon-air flames typically have a large Markstein number and therefore admit a restabilisation zone on a larger range of frequencies. Here, we perform lean propane-air flame experiments with three different equivalence ratios. The experiment is performed several times for each flame, adjusting the shaker intensity between each run. This is done in order to find the appropriate value to reach the parametric instability threshold in the very vicinity of the antinode of the mode. This setup allows the generation of flow oscillations that go from $\widetilde{u}_a \approx 0$ (nodes) to $\widetilde{u}_a = \widetilde{u}_{II}^*$ (antinodes). In this way, the flame experiences all of the interesting $\widetilde{u}_a$ range during its propagation. Here, we perform the threshold measurements for different flames at different forcing frequencies. The results are then compared to theoretical values. To compute these theoretical thresholds, the laminar flame speeds are taken from Bosschaart and de Goey [31], the expansion ratios are taken from a numerical resolution of the flame structure using the Cantera software [32] with a complex chemical-kinetic SanDiego mechanism [33] and the Markstein numbers are taken from Searby and Quinard [34]. The resulting set of parameters is summarized in table I and here:

$$D_{th} = 2 \times 10^{-5} m^2.s^{-1}, \qquad g = 9.81 m.s^{-2}, \qquad Pr = 0.9, \tag{16}$$

$$d_L = D_{th}/u_L, \qquad \tau_L = D_{th}/u_L^2, \qquad \widetilde{\omega}_a = 2\pi\tau_L f_{shaker}, \qquad Fr = u_L/\sqrt{g d_L}. \tag{17}$$

The first thing to observe as a qualitative comparison between theory and experiments is the existence or absence of a stabilization zone (i.e $u_I^* < u_{II}^*$). For each type of experiment, this conclusion has been summarized in the last two

φ	f_{shaker}	$\widetilde{\omega}_a$	u_L	γ	Ma	Fr	λ_2	$\mathcal{J}$	$\mathcal{H}$	Rest	Rest th
0.8	$63Hz$	0.096	$0.28m.s^{-1}$	0.854	4.28	10.58	2.62	1.62	0.69	y	y
0.8	$116Hz$	0.186	$0.28m.s^{-1}$	0.854	4.28	10.58	2.62	1.62	0.69	y	y
0.8	$156Hz$	0.250	$0.28m.s^{-1}$	0.854	4.28	10.58	2.62	1.62	0.69	y	y
0.8	$400Hz$	0.641	$0.28m.s^{-1}$	0.854	4.28	10.58	2.62	1.62	0.69	y	y
0.9	$63Hz$	0.058	$0.36m.s^{-1}$	0.863	4.21	15.42	2.7	1.7	0.72	n	n
0.9	$400Hz$	0.388	$0.36m.s^{-1}$	0.863	4.21	15.42	2.7	1.7	0.72	y	y
1.0	$63Hz$	0.047	$0.40m.s^{-1}$	0.868	3.69	18.06	2.75	1.75	0.74	n	n
1.0	$400Hz$	0.314	$0.40m.s^{-1}$	0.868	3.69	18.06	2.75	1.75	0.74	n	y

Table I. Parameters corresponding to each experiments. The equivalence ratio φ is prescribed using Bronkhorst mass flow regulators. The forcing frequency f_{shaker} is prescribed by adjusting the shaker frequency. The non-dimensional angular frequency $\widetilde{\omega}_a$ is computed as $\widetilde{\omega}_a = 2\pi f_{shaker}\tau_L$. The laminar flame speed u_L is taken from [31]. The expansion parameter γ is computed using Cantera [32]. The Markstein number Ma is taken from [34]. Finally, $\mathcal{J}$ and $\mathcal{H}$ are computed following their theoretical expression recalled in the main text.

columns of the above table. The columns are noted "y" if $u_I^* < u_{II}^*$ and "n" in the opposite case. The comparison between the "Rest" and the "Rest th" columns, gives the agreement between experiments and theory, respectively. The agreement is satisfying for all the flames we analyzed except for the case where $\varphi = 1.0$ with forcing frequency $f_{shaker} = 400Hz$.

The comparison between experimental and theoretical thresholds is visible on Fig. 5 : it shows the $\widetilde{u}^*$ and the $\widetilde{k}^*$ values for three different equivalence ratios at fixed forcing frequency $f_{shaker} = 400Hz$. Despite the fact that the value for f_{shaker} is fixed, it is important to note that the reduced forcing frequency $\widetilde{\omega}_a$ is not.
For the restabilization threshold, we observe that both the k_I^* and the u_I^* values remain nearly constant when the equivalence ratio is increased (Fig. 5A and 5C). This is in good agreement with the trend predicted by theory (red curve). Looking now at the actual values, we remark that the measured u_I^* values are substantially lower than the ones predicted by theory. On the other hand, the measured k_I^* values are in relatively good agreement.
For the parametric threshold, our measurements indicate that u_{II}^* increases with the equivalence ratio (Fig. 5B) while k_{II}^* (Fig. 5D) decreases. This is not the trend predicted by theory, where u_{II}^* is expected to decrease with the equivalence ratio and k_{II}^* is expected to remain nearly constant for these flames at this forcing frequency.

These data and additional ones at other forcing frequencies f_{shaker} are also reported on Fig. 4 in term of the non-dimensional forcing frequency $\widetilde{\omega}_a$. As mentioned in the previous section, the theoretical thresholds on this figure have been computed for 3 different Markstein numbers and with all the other parameters corresponding to a Propane-air flame with equivalence ratio $\varphi = 0.8$. As $Ma = 4.28$ corresponds to the Marsktein value associated with this type of flame (see table I), we theoretically expect the experimental data associated with equivalence ratio $\varphi = 0.8$ to collapse on the theoretical red curve $Ma = 4.28$. The two other equivalence ratios studied in the present experiments are not expected to collapse on any of the theoretical curves as they not only have a different Markstein number but also different Fr, $\mathcal{J}$ and $\mathcal{H}$. However, we shall see that analyzing the trend of the evolution of their thresholds with $\widetilde{\omega}_a$ provides interesting information.

Among the flames studied here, complete restabilization is observed only for the flame with an equivalence ratio $\varphi = 0.8$ (at all the forcing frequencies studied here) and for the flame $\varphi = 0.9$ at low frequency. For the case $\varphi = 0.8$, the restabilization threshold remains nearly constant when $\widetilde{\omega}_a$ is increased both in terms of acoustic speed ($\widetilde{u}_I^*$) and wavenumber ($\widetilde{k}_I^*$). This trend is in good agreement with the theoretical results that predict a constant restabilization threshold except in a thin boundary layer at low forcing frequency where both $\widetilde{u}_I^*$ and $\widetilde{k}_I^*$ decrease drastically (Fig. 4A and 4C). We note that this boundary layer is not observed in our experimental data. Comparing the actual values of these thresholds with the theoretical ones, we note that the agreement is satisfying for the wavenumbers (Fig. 4C) but not for the acoustic forcing speed (Fig. 4A), where the measured thresholds are substantially lower than the expected ones.

Looking now at the results obtained for the parametric instability threshold (Fig. 4B and 4D), we observe that for the three equivalence ratios studied here the measured values for $\widetilde{u}_{II}^*$ remain nearly constant when $\widetilde{\omega}_a$ is increased while the theory predicts a linearly increasing threshold value if Ma remains constant (red curves Fig. 4B). For the wavenumbers, we observe that $\widetilde{k}_{II}^*$ increases with the forcing frequency for the three equivalence ratios analyzed here (Fig. 4D). This tendency is in relatively good agreement with what the theory predicts, although the experimental data seem to increase faster than the theoretical.

V. DISCUSSION

The experimental measurements presented in the previous section display major discrepancies with the theoretical predictions given by the Searby & Rochwerger theory. In particular, for the restabilization threshold, the agreement on the wavenumber values $\widetilde{k}_I^*$ is satisfying (Fig. 4C and 5C). However, while the experimental values for $\widetilde{u}_I^*$ (Fig. 4A and 5A) show the correct trend (except at very low frequency), the measured values are substantially lower than the ones predicted by theory. This large discrepancy cannot be explained by a misestimation of the actual Ma and/or $\widetilde{\omega}_a$ associated with the experimental flame, as this threshold is not very dependent on these two quantities (see parametric study carried out in §III B). Moreover, as pointed out earlier, while some discrepancies are observed on $\widetilde{u}_I^*$, the agreement on $\widetilde{k}_I^*$ is satisfying. Here we argue that heat losses might be responsible for the discrepancy observed between experiments and theory on the restabilization threshold. Indeed, (2) was obtained under an adiabatic hypothesis. In our apparatus, the flame is confined between two walls and the heat losses play an important role in the dynamics [35]. Heat losses were shown to inhibit the standard Darrieus-Landau instability [2]. With the present type of burner, they were shown to affect the entire range of unstable wave numbers quite uniformly. Mathematically, this corresponds to the addition of a negative growth rate to the entire range of unstable wavelengths [35]. A flame in this apparatus is therefore less unstable than its adiabatic counterpart and is easier to restabilize (i.e it requires a smaller forcing amplitude $\widetilde{u}_a$ to observe restabilization). This explains the smaller values of $\widetilde{u}_I^*$ measured in our experiments. Meanwhile, as these heat losses are affecting all the wavenumbers uniformly, a good agreement on $\widetilde{k}_I^*$ is expected with the adiabatic theory. This is what we observe in our experiments (Fig. 3C and 4C). Finally, the steep decrease of both $\widetilde{u}_I^*$ and $\widetilde{k}_I^*$ predicted by theory and not observed with our experimental data (Fig. 4A and 4C) can also be explained by heat losses. Heat losses tend to decrease the actual u_L and therefore, by using the adiabatic u_L from [31] to non dimensionalize the forcing frequency, we are underestimating the actual $\widetilde{\omega}_a$ associated with our experimental flames. This means that the experimental data on Fig. 4A and 4C should be shifted horizontally towards higher $\widetilde{\omega}_a$ values and are probably already in the frequency range where $\widetilde{u}_I^*$ and $\widetilde{k}_I^*$ are frequency independent. To validate this hypothesis, in future works, it might be interesting to search for this boundary layer predicted by theory at low frequency by forcing these flames with lower frequencies. This could be achieved in a Hele-Shaw burner that uses walls with a lower fundamental frequency (for example using plastic walls instead of glass walls).

Concerning the parametric threshold $(\widetilde{u}_{II}^*, \widetilde{k}_{II}^*)$, the theory does not even describe the correct trend observed in our experimental measurements. In particular, $\widetilde{u}_{II}^*$ is expected to increase linearly with the forcing frequency. In our experiments we have observed that the thresholds remain nearly constant when the frequency is increased. The theoretical red curves are computed for a constant Ma number, but the actual Markstein value associated with our experimental flames is apparently changing when the forcing frequency is increased. According to Joulin's theory, the Lewis component is disappearing when the acoustic time is no longer small compared to the transit time. For these lean propane air flames, this corresponds to Markstein values that decrease when the frequency is increased. This is exactly what we observe with our measurements. For the speed $\widetilde{u}_{II}^*$, the threshold remains nearly constant instead of growing linearly because Ma is decreasing with frequency. In practice it corresponds to a flame starting at a darker red curve (high Markstein value) and moving towards the lighter red curves (lower Markstein values). This is corroborated by the $\widetilde{k}_{II}^*$ measurements that display a steeper slope than the theoretical curves for the same reason: the flames are evolving from the darker red curves to the lighter ones when the frequency is increased (see Fig. 4B and 4D). This would also explain the incorrect trend observed when the dimensional forcing frequency f_{shaker} is fixed and the equivalence ratio φ is varied. For this lean propane-air flames both Ma and $\widetilde{\omega}_a$ are decreasing when the equivalence ratio is increased from $\varphi = 0.8$ to $\varphi = 1.0$. At fixed Ma, based on theory, $\widetilde{u}_{II}^*$ is expected to increase with $\widetilde{\omega}_a$ (see Fig. 4B). At fixed frequency, $\widetilde{u}_{II}^*$ is expected to increase with Ma. By decreasing Ma and $\widetilde{\omega}_a$, we therefore have two different effects that are supposed to make $\widetilde{u}_{II}^*$ decrease, which explain the theoretical trend observed on Fig. 5B. However, if Ma is indeed decreasing with $\widetilde{\omega}_a$ as expected by Joulin's theory, it means that we are overestimating Ma by taking the low frequency value obtained in [10, 11] and therefore overestimating u_{II}^*. At fixed f_{shaker}, $\widetilde{\omega}_a$ is higher at $\varphi = 0.8$ than at higher equivalence ratio and we are therefore overestimating Ma by a larger amount. This leads in turn to a larger overestimation of u_{II}^* than at a higher equivalence ratio, as observed on Fig. 5.

Finally, we note that our experiments are compared to linear stability analysis although no total restabilization zone could be observed in some cases ($(\varphi = 0.9, f_{shaker} = 63Hz)$, $(\varphi = 1.0, f_{shaker} = 63Hz)$ and $(\varphi = 1.0, f_{shaker} = 400Hz)$). In those cases, where the parametric instability does not appear from a flat front but from a Darrieus-Landau wrinkled one (see Fig. 2H), the oscillator model described by (2) is no longer valid and non-linear effects could have a non-negligible influence on the threshold values (see [36, 37]).

VI. CONCLUSION

In this paper, the flame interaction with a periodic time dependent flow has been studied experimentally using the flame/structure coupling uncovered in [23]. The measured parametric restabilization and destabilization thresholds have been compared to those given by the theory introduced in Searby and Rochwerger [13]. Both the u_I^* and u_{II}^* values from our experiments are much smaller than those predicted by theory. However, the agreement on k_I^* and k_{II}^* is surprisingly good. This trend has been attributed to thermal losses which lower the DL growth rate quite uniformly over the range of unstable wavenumbers. In addition, our measurements suggest a nearly constant parametric threshold when the forcing frequency $\widetilde{\omega}_a$ is increased. This is in contradiction with theory, which predicts a linear increase of $\widetilde{u}_{II}^*$ with $\widetilde{\omega}_a$. This disagreement may be explained by a decrease of the Markstein number when the frequency increases, as predicted in [2] (for flames with $Le > 1$) and already observed experimentally and numerically in previous studies [13, 14, 38]. Our results constitute a confirmation of the results obtained in these former studies in a completely different kind of apparatus and suggest that frequency dependent Markstein numbers should be used in combustion models for time dependent flows.

VII. ACKNOWLEDGEMENTS

We thank Daniel Mazzoni for his implication in the experimental facility. We thank the Excellence Initiative of Aix-Marseille University - A*MIDEX, and Labex MEC, for funding.

[1] P. Clavin and G. Joulin, "Flamelet library for turbulent wrinkled flames," in *Turbulent Reactive Flows*, edited by R. Borghi and S. N. B. Murthy (Springer US, 1989) p. 213–240.
[2] G. Joulin and G. Sivashinsky, "Influence of Momentum and Heat Losses on the Large-Scale Stability of Quasi-2D Premixed Flames," Combustion Science and Technology **98**, 11–23 (1994).
[3] J. K. Bechtold and M. Matalon, "The dependence of the Markstein length on stoichiometry," Combustion and Flame **127**, 1906–1913 (2001).
[4] P. Clavin and J. C. Graña-Otero, "Curved and stretched flames: the two markstein numbers," Journal of Fluid Mechanics **686**, 187–217 (2011).
[5] P. Pelcé and P. Clavin, "Influence of hydrodynamics and diffusion upon the stability limits of laminar premixed flames," Journal of Fluid Mechanics **124**, 219 (1982).
[6] M. Matalon and B. J. Matkowsky, "Flames as gasdynamic discontinuities," Journal of Fluid Mechanics **124**, 239 (1982).
[7] P. Clavin and P. Garcia, "The influence of the temperature dependence of diffusivities on the dynamics of flame fronts," J. Méc. Théor. Appl **2**, 245–263 (1983).
[8] Guy Joulin, "On the response of premixed flames to time-dependent stretch and curvature," Combustion Science and Technology **97**, 219–229 (1994).
[9] Paul Clavin and Guy Joulin, "High-frequency response of premixed flames to weak stretch and curvature: a variable-density analysis," Combustion Theory and Modelling **1**, 429–446 (1997).
[10] S. G. Davis, Joël Quinard, and Geoffrey Searby, "Determination of Markstein numbers in counterflow premixed flames," Combustion and Flame **130**, 112–122 (2002).
[11] S.G. Davis, J. Quinard, and G. Searby, "Markstein numbers in counterflow, methane- and propane- air flames: a computational study," Combustion and Flame **130**, 123–136 (2002).
[12] G. H. Markstein, "Interaction of Flow Pulsations and Flame Propagation," Journal of the Aeronautical Sciences **18**, 428–429 (1951).
[13] G. Searby and D. Rochwerger, "A parametric acoustic instability in premixed flames," Journal of Fluid Mechanics **231**, 529–543 (1991).
[14] B. Denet and A. Toma, "Numerical Study of Premixed Flames Parametric Acoustic Instability," Combustion Science and Technology **109**, 23–33 (1995).
[15] M. M. Alexeev, O. Y. Semenov, and S. E. Yakush, "Experimental Study on Cellular Premixed Propane Flames in a Narrow Gap between Parallel Plates," Combustion Science and Technology , 1–20 (2018).
[16] Hye Jin Jang, Gyu Min Jang, and Nam Il Kim, "Unsteady propagation of premixed methane/propane flames in a mesoscale disk burner of variable-gaps," Proceedings of the Combustion Institute **37**, 1861–1868 (2019).
[17] Elias Al Sarraf, Christophe Almarcha, Joël Quinard, Basile Radisson, Bruno Denet, and Pedro Garcia-Ybarra, "Darrieus–Landau instability and Markstein numbers of premixed flames in a Hele-Shaw cell," Proceedings of the Combustion Institute **37**, 1783–1789 (2019).
[18] C. Almarcha, B. Radisson, E. Al Sarraf, E. Villermaux, B. Denet, and J. Quinard, "Interface dynamics, pole trajectories, and cell size statistics," Physical Review E **98** (2018).

[19] F. Veiga-López, D. Martínez-Ruiz, E. Fernández-Tarrazo, and M. Sánchez-Sanz, "Experimental analysis of oscillatory premixed flames in a Hele-Shaw cell propagating towards a closed end," Combustion and Flame **201**, 1–11 (2019).

[20] Fernando Veiga-López, Mike Kuznetsov, Daniel Martínez-Ruiz, Eduardo Fernández-Tarrazo, Joachim Grune, and Mario Sánchez-Sanz, "Unexpected propagation of ultra-lean hydrogen flames in narrow gaps," Physical Review Letters **124**, 174501 (2020).

[21] B. Radisson, B. Denet, and C. Almarcha, "Nonlinear dynamics of premixed flames: from deterministic stages to stochastic influence," Journal of Fluid Mechanics **903**, A17 (2020).

[22] Ajit Kumar Dubey, Yoichiro Koyama, Nozomu Hashimoto, and Osamu Fujita, "Exploring a critical diameter for thermo-acoustic instability of downward propagating flames in tubes," Proceedings of the Combustion Institute **38**, 1945–1954 (2021).

[23] Basile Radisson, Juliette Piketty-Moine, and Christophe Almarcha, "Coupling of vibro-acoustic waves with premixed flame," Physical Review Fluids **4**, 121201 (2019).

[24] Norman William McLachlan, "Theory and application of Mathieu functions," Publisher to the University Geoffrey Cumberlege, Oxford University Press (1951).

[25] Geoffrey Searby and Daniel Rochwerger, "A parametric acoustic instability in premixed flames," Journal of Fluid Mechanics **231**, 529–543 (1991).

[26] F. A. Alhargan, "A complete method for the computations of Mathieu characteristic numbers of integer orders," SIAM Review **38**, 239–255 (1996).

[27] J. Yanez, M. Kuznetsov, and R. Redlinger, "The acoustic–parametric instability for hydrogen–air mixtures," Combustion and Flame **160**, 2009–2016 (2013).

[28] Ajit K. Dubey, Yoichiro Koyama, Sung Hwan Yoon, Nozomu Hashimoto, and Osamu Fujita, "Range of "complete" instability of flat flames propagating downward in the acoustic field in combustion tube: Lewis number effect," Combustion and Flame **216**, 326–337 (2020).

[29] F. Baillot, D. Durox, S. Ducruix, G. Searby, and L. Boyer, "Parametric Response of a Conical Flame to Acoustic Waves," Combustion Science and Technology **142**, 91–109 (1999).

[30] V. V. Bychkov, "Analytical scalings for flame interaction with sound waves," Physics of Fluids **11**, 3168–3173 (1999).

[31] K. J. Bosschaart and L. P. H. de Goey, "The laminar burning velocity of flames propagating in mixtures of hydrocarbons and air measured with the heat flux method," Combustion and Flame **136**, 261–269 (2004).

[32] D. G. Goodwin, H. K. Moffat, and R. L. Speth, "Cantera: An Object-oriented Software Toolkit for Chemical Kinetics, Thermodynamics, and Transport Processes," (2017), 10.5281/zenodo.170284, version 2.3.0.

[33] "San Diego Mechanism: Chemical-Kinetic Mechanisms for Combustion Applications," http://combustion.ucsd.edu (2016).

[34] G Searby and J Quinard, "Direct and indirect measurements of Markstein numbers of premixed flames," Combustion and Flame **82**, 298–311 (1990).

[35] Basile Radisson, Bruno Denet, and Christophe Almarcha, "Nonlinear dynamics of flame fronts with large-scale stabilizing effects," Phys. Rev. E **103**, 063104 (2021).

[36] R. A. Rego, Y. D'Angelo, and G. Joulin, "On nonlinear model equations for the response of premixed flames to acoustic like accelerations," Combustion Theory and Modelling **17**, 53–75 (2013).

[37] R. C. Assier and X. Wu, "Linear and weakly nonlinear instability of a premixed curved flame under the influence of its spontaneous acoustic field," Journal of Fluid Mechanics **758**, 180–220 (2014).

[38] J. B. Chen and H. G. Im, "Stretch effects on the burning velocity of turbulent premixed hydrogen/air flames," Proceedings of the Combustion Institute **28**, 211–218 (2000).